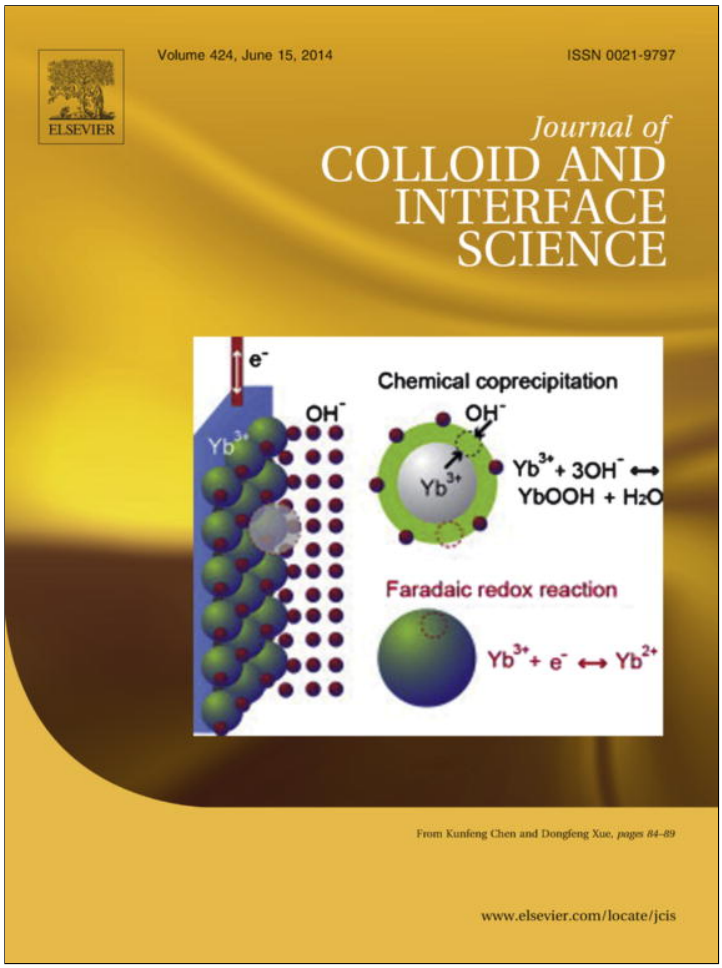

Journal of Colloid and Interface Science 424 (2014) 90–97

Contents lists available at ScienceDirect

Journal of Colloid and Interface Science

www.elsevier.com/locate/jcis

Replacement of CTAB with peptidic ligands at the surface of gold nanorods and their self-assembling properties

C. Hamon [a], T. Bizien [a,b], F. Artzner [b], P. Even-Hernandez [a], V. Marchi [a,*]

[a] Institut des Sciences Chimiques de Rennes, University Rennes 1, UMR 6226 C.N.R.S., Campus de Beaulieu, 35042 Rennes Cedex, France
[b] Institut de Physique de Rennes, University Rennes 1, UMR 6251 C.N.R.S., Campus de Beaulieu, 35042 Rennes Cedex, France

ARTICLE INFO

Article history:
Received 9 January 2014
Accepted 1 March 2014
Available online 13 March 2014

Keywords:
Peptide
Gold nanorods
Self-assembly
Ligand exchange
Ordered structure
Smectic B order
Small Angle X-ray Scattering

ABSTRACT

Herein, we describe the self-assembling of gold nanorods (GNRs) induced during the ligand exchange at their surface. An exchange reaction between tricysteine PEGylated peptidic ligands and cetyltrimethylammonium bromide (CTAB)-protected gold nanorods is conducted. We demonstrated that the terminal group charge (positively or negatively charged) and the hydrophobicity of the peptidic ligands (bearing or not an undecanoyl chain) strongly affects the self-organization of the GNRs occurring in solution. Adjusting the amount of short PEGylated peptides causes a self-organization of the gold nanorods in solution, resulting in a red- or blue-shift of the plasmon bands. The decrease of their surface charge and the self-assembling in solution were first shown by zetametry, by Dynamic Light Scattering and UV-spectroscopy. Thanks to Small Angle X-ray Scattering experiments and Transmission Electron Microscopy images, the self-organization of the nanorods in solution was clearly demonstrated and correlated to the spectroscopic change in absorbance. Conversely, in the case of longer PEGylated peptidic ligands including an undecanoyl chain, the GNRs are particularly stable against aggregation for several days after purification. By controlled drying on a substrate, we showed their ability to self-organize into well-defined ordered structures making them very attractive as building blocks to design optical materials.

1. Introduction

Metallic anisotropic gold nanorods (GNRs) exhibit original absorption properties of Surface Plasmon Resonance (SPR) depending on their aspect ratio [1]. Due to their intrinsic shape anisotropy, the GNRs exhibit transverse and longitudinal SPR modes corresponding to the coherent oscillation perpendicular and parallel to the long GNR axis respectively. In addition they tend to self-assemble in a side-by-side or end-to-end manner because of their anisotropic shape [2]. These individual and ensemble optical properties, resulting from plasmonic coupling, make them promising candidates as building blocks for optical materials and biological sensing [7,8]. The absorption properties of the GNRs in an ensemble strongly depend on the nanorods interdistance but also on the mutual orientation of the GNRs with respect to each other [3].

To control the self-assembling of GNRs, finely tuning of the surface chemistry is of foremost importance to find a compromise between attractive and repulsive interactions. We previously demonstrated that 3D crystals of gold nanorods with a local smectic B order could be obtained thanks to a fine control of the surface chemistry [4]. In the classical protocols described for GNRs synthesis, crude GNRs are coated by an interdigitated CTAB bilayer [5]. This surfactant is responsible for both directing the rod shape during the synthesis and maintaining colloidal stability due to repulsive electrostatic interactions. Nevertheless CTAB is not suitable for biosensing applications due to its surfactant cytotoxicity (CMC 1 mM) and the lack of colloidal stability of CTAB gold nanorods in saline buffers [6]. As CTAB is particularly hard to remove, many different strategies have been employed. Replacing CTAB by PEGylated thiolates has been widely used [4,5d,6d,7]. Another pathway involves the replacement of CTAB ligands with hydrophobic thiols thanks to a round-trip phase transfer ligand exchange [8]. It is also possible to encapsulate the positively charged GNRs with negatively charged polyelectrolyte [9]. An alternative approach is to synthesize directly gold nanoparticles with the ligands of interest [10]. However it remains a challenging task to obtain a controlled shape of nanoparticles by such way. Furthermore peptides capped GNRs are promising for applications in biological media to target cells and proteins combining the biological interest of the peptide

Abbreviations: GNR, gold nanorods; SAXS, Small Angle X-ray Scattering; TEM, Transmission Electron Microscopy; CTAB, cetyl trimethyl ammonium bromide; SPR, Surface Plasmon Resonance; DMSA, dimercapto succinic acid; TBE buffer, Tris-Borate-EDTA buffer; DLS, Dynamic Light Scattering.

* Corresponding author.
E-mail address: valerie.marchi@univ-rennes1.fr (V. Marchi).

http://dx.doi.org/10.1016/j.jcis.2014.03.002
0021-9797/

[11] to the optical properties of metallic nanoparticle [5d]. They are mainly biocompatible and it is easy to adjust the terminal group with the peptide sequence. Peptides have been previously used to functionalize gold nanoparticles [12]. There are only a few examples of peptides grafting directly on gold nanorod surface in the literature [6b]. Indeed most of the described tentatives to graft peptides consist in a two-steps strategy: first the CTAB is replaced with PEGylated ligands and second a peptide of interest is grafted *via* an amide coupling or *via* a linker [12b,13]. Here we describe the functionalization of the GNRs with peptides following a one-step strategy. So this direct method gives better yields of chemical functionalization and avoids to intermediately purify nanoparticles. Additionally this one-step strategy permits also to control the number of functional sites grafted to the GNR surface and reduces the ratio of lost nanoparticles during the washing steps of the functionalization. In view to manipulate and control the interactions between GNRs in aqueous solution, we selected here PEGylated peptidic polycystein ligands to functionalize gold nanorods because of their high affinity for gold surface as well as their chemical versatility and easy accessibility. One thiol is commonly used to graft on gold surfaces and is enough to form a stable coating [10]. Herein we used a set of peptidic ligands all bearing an adhesion domain composed of three cysteins that reinforces the interaction with GNR surface in comparison to only one cystein. The resulting strong grafting could improve the long-term colloidal stability compared with GNRs modified with mono-thiol ligands. The peptidic ligands can be used to functionalize other types of surfaces, for example CdSe/ZnS quantum dots [14]. In addition, the charge of these peptidic ligands can be easily varied with different terminal groups such as aspartic or lysine amino acids. Their hydrophobicity can also be modified thanks to an undecanoyl chain.

Here we show that the ligand exchange between CTAB and small peptidic ligands induces the self-assembling of the GNRs in solution depending on their surface charge. Self-assembling of GNRs has been previously described in the literature to make sensors for toxin [15]. or DNA detection [16] based on specific interaction. Moreover screening of the repulsive electrostatic interaction between CTAB coated GNRs was obtained by using anionic salts such as dimercaptosuccinic acid (DMSA) [17], EDTA [18], sodium citrate [3c] or adipic acid [19] interacting directly with the CTAB cationic cetyl trimethyl ammonium head-groups. Here we investigated the electrostatic-driven self-assembling of GNRs in solution induced by adjusting the amount of peptidic ligands and changing their charge. The formation of the GNRs self-assembly was followed by the evolution of the optical properties and analyzed by Dynamic Light Scattering, zetametry and transmission electronic microscopy. Finally the technique of Small Angle X-ray Scattering (SAXS) gives direct access to the aggregates structure in solution. We found that the structures were strongly affected by the amount of peptidic ligands during the exchange with CTAB and are correlated with the observed optical changes. The nanorods surface charge was found to direct the size and the morphology of the aggregates. In addition the hydrophobicity of the peptidic ligands strongly affects their self-organization properties in solution. Interestingly in the case of the long undecanoyl peptidic ligands, the obtained peptidic GNRs are very stable in aqueous suspension after elimination of the ligand excess. This latter observation highlighted the importance of the alkyl chain to organize the organic shell coating a nanoparticle [13a,20]. Besides their very high stability against aggregation, we show that self-assemblies of the GNRs can be induced by drying them from water suspension. This last result makes promising those GNRs as building blocks to design optical materials.

2. Materials and methods

2.1. Materials and instrumentation

Silver nitrate, sodium borohydride, hexadecyltrimethylammonium bromide, gold(III) chloride hydrate, L-ascorbic acid used in the gold nanorods syntheses were purchased from Sigma. The peptides (C_3E_6D, C_3E_6, C_3E_6K, $C_3A_{11}E_4$, $C_3A_{11}E_4CO_2H$) were synthetized and purified by HPLC (>90%) by polypeptide (Strasbourg, France). The absorbance measurements were performed on a Cary 100 Scan UV–Visible Spectrophotometer, Varian, Australia. The TEM measurements were performed using a JEOL 1400 with an acceleration voltage of 200 kV. Dynamic Light Scattering (DLS) and zetametry were performed on a Zetasizer Nano-ZS ZEN3600 (Malvern Instrument, UK). IR spectroscopic characterizations were carried out on a Varian 640-IR FTIR ATR spectrometer.

2.2. Methods

2.2.1. Electrophoresis

Agarose gels (Agarose 'For Routine Use', Sigma) were prepared with 0.5% agarose (m/m water) and immersed in TBE buffer (45.5 mM Tris-Borate, 1 mM EDTA, pH = 8.3, Sigma). The gels were placed in a horizontal electrophoresis system (X_LUltra™ V-2 Labnet International, USA) with electrode spacing of 15 cm. Before loading the gel with the PEGylated peptide nanoparticle samples, a small amount of loading buffer (30% Glycerol in 0.5× TBE-buffer) was added to each sample in order to increase the viscosity in the well.

2.2.2. Zeta potential

All the samples were filtered on 0.22 μm Millipore (Millex GV, Sigma–Aldricht, France) to avoid dust in samples. The samples were introduced into PMMA micro cells (Zetasizer, nano-series) and solutions were loaded with a 10 mM NaCl buffer.

2.2.3. Fourier Transform Infra-Red Spectroscopy (FTIR)

CTAB and peptide powder were directly deposited on the ATR crystal. GNRs capped with the peptidic ligands were purified by using membrane dialysis (cut off: 50,000 MWCO) in presence of a mixed bed resin (Sigma). Typically, 1 mL of GNR suspension capped by peptide (2.72 nM) was introduced into the dialysis bag and was then placed in 1 L water containing 10 g of ion exchange resin for suspension 1 h under stirring. This procedure was repeated 3 times to remove the excess of ligand in solution. The solution was then lyophilised (H-ETO Power Dry PL 300).

2.2.4. GNRs synthesis and peptidic ligand exchange

Gold nanorods have been synthesized *via* a seedless method described here [21]. Briefly, a 10 mL solution containing 3.5 mM aqueous tetrachloroauric acid, 0.2 M CTAB and 1 mM $AgNO_3$ is constituted. Next, 0.12 mL of 0.4 M ascorbic acid was added under stirring. Finally, 64 μL of an ice-cold aqueous 1.6 mM sodium borohydride solution was added. In this procedure, gold nanorods with absorption maximum at 750 nm are obtained 20 min after adding sodium borohydride. For further experiments, the excess of CTAB was removed by two cycle of centrifugation (14000*g*) at room temperature. After each cycle, the supernatant was removed and the pellet containing GNRs is diluted to reach a final ligand concentration of CTAB of 0.5 mM. The nanorod concentration was derived from the optical density measured at 750 nm and the extinction coefficient provided in the literature [6d]. The titer of this stock solution of "as-synthesized" GNRs was found to be 0.4 nM. For the peptides conjugation, 10 μL of a 10 mM peptide solution is added to 1 mL of gold nanorods, the mixture was vortexed and

then left to react for 24 h. The global peptide concentration during the ligand exchange is 10 μM. Then GNRs suspension was purified on size exclusion column (Sephadex Nap-5, GE Healthcare) with 10 mM NaCl solution as eluent to remove the excess of peptide.

2.2.5. Transmission Electronic Microscopy (TEM)

Samples were deposited on a formvar carbon grid (300 mesh copper, Agar Scientific). Typically, a 5 μL GNRs suspension (10^{-9} M) was deposited on the TEM grid and was left drying for 2 h.

2.2.6. Small Angle X-ray Scattering (SAXS)

SAXS measurements were performed on the high brilliance SWING beamline (12 keV) located at the Soleil synchrotron facility. All samples exhibited powder diffraction patterns; thus, circular integration allowed one to plot the scattering intensity as a function of the radial wave vector $q = 4\pi \sin(\theta)/\lambda$. Self-assembled condensed phases were prepared in 1.3–1.6 mm diameter glass capillaries (Glas-Technik & Konstruktion Müller & Müller OHG). Typically, the GNR suspension was at an initial concentration of 10^{-8} M. It was prepared in 0.5 mM CTAB and the capillaries were sealed.

3. Results and discussion

3.1. Synthesis and functionalization of the gold nanorods (GNRs)

The formation of gold nanorods was obtained after 20 min in presence of the reducing agent (Sodium borohydride) according to described methods [21–22], which does not require gold seeds. After the synthesis, the GNRs were coated with an interdigitated CTAB bilayer giving rise to a positive surface charge of the nanorods [5c]. Only a few spheres were visible on TEM images as shown in Fig. S1. The size of the nanorods was estimated from TEM images. The mean diameter was found around 8 ± 3.5 nm and the mean length around 23 ± 7 nm. The GNRs were characterized by two maxima in the UV/Vis spectrum (see Fig. 2): the Longitudinal Surface Plasmon (LSP) mode in the NIR region with a position at 750 nm and the Transversal Surface Plasmon (TSP) mode occurring around 510 nm. After two successive cycles of centrifugation–precipitation to remove the CTAB excess, the final concentration of CTAB was fixed at 0.5 mM.

To exchange the ligands, the nanorods were then incubated in the presence of an excess of the desired PEGylated peptidic ligands (Fig. 1a and b). In view to reinforce their affinity, all the used peptides possess a tricystein (C_3) sequence as multivalent thiol anchor to the gold surface ([1]red part on Fig. 1b). The presence of a hexa-ethylene-oxy spacer noted E_6 increases the accessibility of the terminal groups in the aqueous environment and introduces a repulsive osmotic force due to the unfavourable entropy associated with confining the E_6 chains between two NP surfaces (blue part on Fig. 1b). This steric repulsion leads to a reduction the Van der Waals interactions between colloids [23]. Finally different charged chemical functions can be grafted as terminal groups (green part on Fig. 1b): negatively charged aspartic (C_3E_6D), positively charged lysine (C_3E_6K) or neutral (C_3E_6). Also the $C_3A_{11}E_4CO_2H$ and $C_3A_{11}E_4$, peptides (Fig. 1c) have been tested to evaluate the contribution of the attractive van der Waals interactions between the alkyl chains to stabilize a monolayer of ligands and increase the colloidal stability of the GNRs. These two peptides present the same anchor group (red part on Fig. 1c), an additional undecanoyl chain (noted A_{11}) and two different terminal groups (green part Fig. 1c): negatively charged carboxylic group

[1] For interpretation of color in Fig. 1, the reader is referred to the web version of this article.

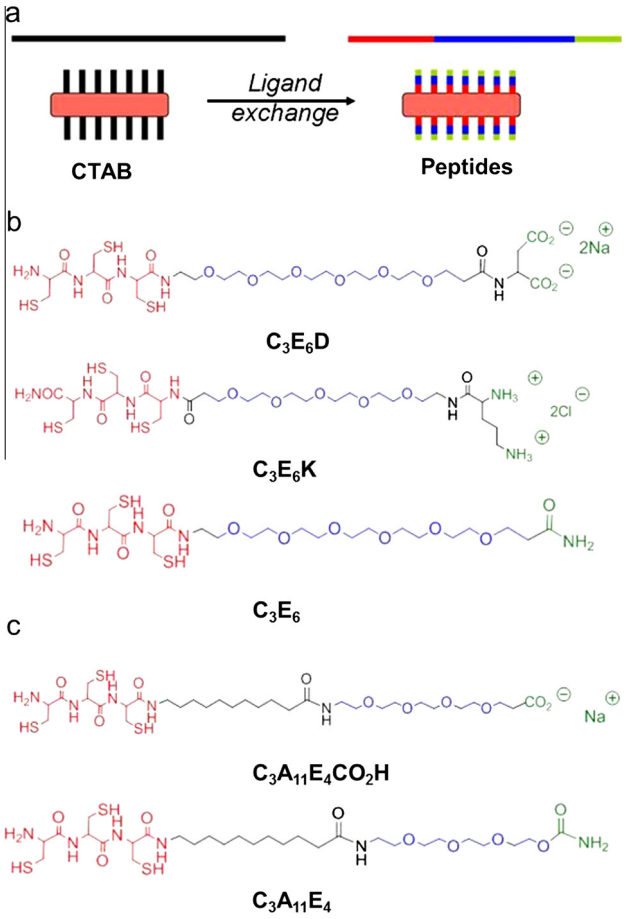

Fig. 1. (a) Schematic view of the ligand exchange process on GNRs. Chemical structures of the peptides used for ligand exchange: (b) short PEGylated peptidic ligands of different charges: negatively (C_3E_6D), positively charged (C_3E_6K) and neutral (C_3E_6). (c) Long PEGylated peptidic ligands with an undecanoyl chain as hydrophobic spacer either negatively charged $C_3A_{11}E_4CO_2H$ or neutral ($C_3A_{11}E_4$).

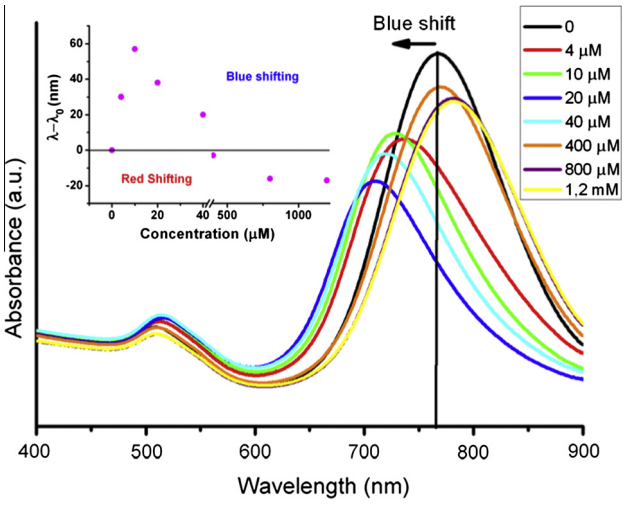

Fig. 2. UV–Vis spectra during the titration of a GNRs suspension (10^{-9} M) with increasing amounts of C_3E_6D. The resulting spectra have been recorded after two hours of incubation with C_3E_6D. Insert: Corresponding shift of λ^{max} of the LSPR band during the titration by taken as reference the initial value λ_0 of the pure CTAB GNRs suspension.

($C_3A_{11}E_4CO_2H$) and neutral alcohol group ($C_3A_{11}E_4$). These peptides are expected to give rise to a better surface coverage of the GNRs after exchange because of the tendency of the undecanoyl chains to form a densely packed monolayer due to attractive Van der Waals interactions [13a,20].

In the case of C_3E_6D, the obtained peptidic gold nanorods were first analyzed by Fourier Transform Infra-Red (FTIR) spectroscopy (see Fig. S2) after removal of the ligand excess in solution by subsequent membrane dialysis in the presence of an ion exchange resin. This purification step allowed us to investigate the nature of the ligands at the surface of GNRs. The FTIR spectra of the GNRs coated with C_3E_6D are shown in Fig. S2. The presence of the amide carbonyl band at 1546 cm^{-1} clearly demonstrates the binding of C_3E_6D peptide to the GNR surface. In addition the characteristic bands of the C_3E_6D in the region of C–H stretching at 830–720 cm^{-1} were also observed in the C_3E_6D GNRs sample. However the important signals coming from the CH_2 stretching bands (2917 and 2849 cm^{-1}) indicate that CTAB ligands are not completely exchanged.

To validate the efficiency of the chemical functionalization, a biotin-terminated peptide noted $C_3(SG)_3B$ (see its molecular structure in Fig. S3c), bearing a tricystein anchor sequence (see Fig. S3c) and a peptidic serine-glycine spacer was grafted following the same protocol. After removal of the free $C_3(SG)_3B$ peptides, the obtained biotin GNRs were incubated in presence of streptavidin agarose microbeads. After extensive centrifugation-dilution cycles to remove the free GNRs, the agarose microbeads incubated in the presence of the biotin GNRs exhibit the typical color of the GNRs. In the control experiment performed in the presence of the C_3E_6D GNRs, the suspension remains uncolored. This observation is due to the strong biotin/streptavidin molecular recognition and therefore proves the ligand exchange from CTAB to biotin peptide at the GNRs surface.

3.2. Evidence of the GNRs self-assembling during ligand exchange with short PEGylated peptides

During the titration of the gold nanorods with increasing amounts of C_3E_6D, dramatical changes in their optical properties were observed (see Fig. 2). These changes in the optical properties were clearly visible from the color change of the colloidal suspension, which is initially brown, becomes blue and finally turns again to the brown color. We studied first the evolution of the plasmon band-shift in time for an aqueous GNR suspension (10^{-9} M, 0.5 mM CTAB) depending on the amount of C_3E_6D in solution. This kinetic study was performed by UV/Vis spectroscopy for a C_3E_6D concentration of 4 μM and 40 μM. As shown in Figs. S4a and S5a, the spectral shift of the characteristic bands of the GNRs occurs on a short time scale. Indeed after a 2 h time of incubation, the shift of the longitudinal band is stabilized, then only a decrease in the absorbance intensity is observed. We also compare the UV–Vis spectra after 2 h and after 5 days to check that the band shifts observed are stable in time (Figs. S4b and S5b). As shown in Fig. 2, for low peptide concentration, an increasing blue-shift of the Longitudinal Surface Plasmon Resonance (LSPR) band was observed to reach a maximum of 60 nm (see insert in Fig. 2). A final red-shift of 10 nm was observed in presence of a peptidic ligand excess. At the same time, slight red-shift then a blue-shift were observed for the Transversal Surface Plasmon Resonance (TSPR) band by increasing the amount of peptidic ligands. In addition the observed aggregation was also related to the CTAB concentration in solution. In all those experiments the CTAB concentration was fixed below its CMC around 0.5 mM. When the same experiment was performed in a GNR suspension containing 5 mM CTAB no spectral shift in UV–Vis were measured (see Fig. S6). Instead of the blue-shift expected (same peptide amount/concentration as in Fig. S4), we observed only a slight red-shift of the LSPR. This experiment shows the importance of the residual CTAB concentration on the colloidal stability of the GNRs during the ligand exchange process. Similar behavior was observed in the case of the neutral peptide C_3E_6 (see Fig. S7a). In contrast, the titration of the GNRs with the positively charged C_3E_6K peptide (see Fig. S7b) resulted only in a red shift of the LSPR band. This latter observation demonstrates that the original changes in optical properties are correlated with the charges of negative C_3E_6D or neutral C_3E_6 peptidic ligands.

To elucidate the contribution of the surface charge in the interaction between nanoparticles, the grafting of C_3E_6D peptide on GNRs was first followed by agarose gel electrophoresis (see Fig. 3d) according to previously reported protocols [4,14a]. The initial CTAB GNRs were incubated with either a low (blue-shifted sample) or a large (red-shifted sample) amount of C_3E_6D peptides. The two samples were then loaded on electrophoresis gel. Without any purification step, they do not migrate because of the presence of aggregates as suggested by the optical properties. CTAB coated GNRs also do not migrate as expected from their colloidal instability in the presence of a buffer [7]. In the case of the red- and blue-shifted samples, it was possible to eliminate the aggregates by size exclusion chromatography. The purified samples exhibited a migration corresponding to a negative surface charge. This first experiment demonstrates the efficiency of the purification steps to separate the aggregates from the dispersed GNRs and gives access to the final negative surface charge after the ligands exchange with C_3E_6D. To get more quantitative measurements, the mean hydrodynamic diameter and the zeta potential were measured for increasing peptide concentrations. First, in the case of the negatively charged C_3E_6D peptides, aggregates were progressively formed in the solution (see Fig. 3a) whereas the mean zeta potential decreased. A purification step of the GNRs was performed to only measure the contribution of the dispersed nanorods and eliminate the value coming from the excess of positively charged CTAB in solution (see purple curve in Fig. 3a). After removal of the CTAB ligand excess by size exclusion chromatography, the measurements of the zeta potential exhibited a progressive decrease until reaching a plateau corresponding to a final zeta potential of −12 mV (purple, Fig. 3a). These set of experiments clearly demonstrate that a charge reversion of the nanorods occurs during the ligand exchange in agreement with the progressive replacement of CTAB with the peptide. Another set of experiments was performed on nanorods coated with C_3E_6 and C_3E_6K. The evolution of the zeta potential and the mean hydrodynamical diameter are reported in Fig. 3b and c respectively. In the case of the neutral charged peptide C_3E_6, the zeta potential of the suspension decreased of 10 mV and the formation of aggregates was observed for higher amounts of peptides added (Fig. 3b). Conversely, in the case of the positively charged peptide C_3E_6K the zeta potential increases of 10 mV and no aggregation was detected (see Fig. 3c). These latter results clearly confirm the role of electrostatic interaction in self-assembling. The ligand exchange of positively charged CTAB with C_3E_6D and C_3E_6 resulted in a decrease of the surface charge until its reversion. Furthermore the size of the aggregates can be correlated to their optical properties. In the case of oppositely charged peptides, the formation of small aggregates leads to a blue-shift of the LSPR at low peptide concentration whereas a red-shift of the LSPR is observed for larger aggregates at high peptide concentration.

3.3. Investigation of the structures obtained with the short peptide

In view to better understand the correlation between the structures of the aggregates and their optical properties, we investigated the structures of the blue-shifted small aggregates as well as the red-shifted larger ones obtained from C_3E_6D GNRs. Rod-

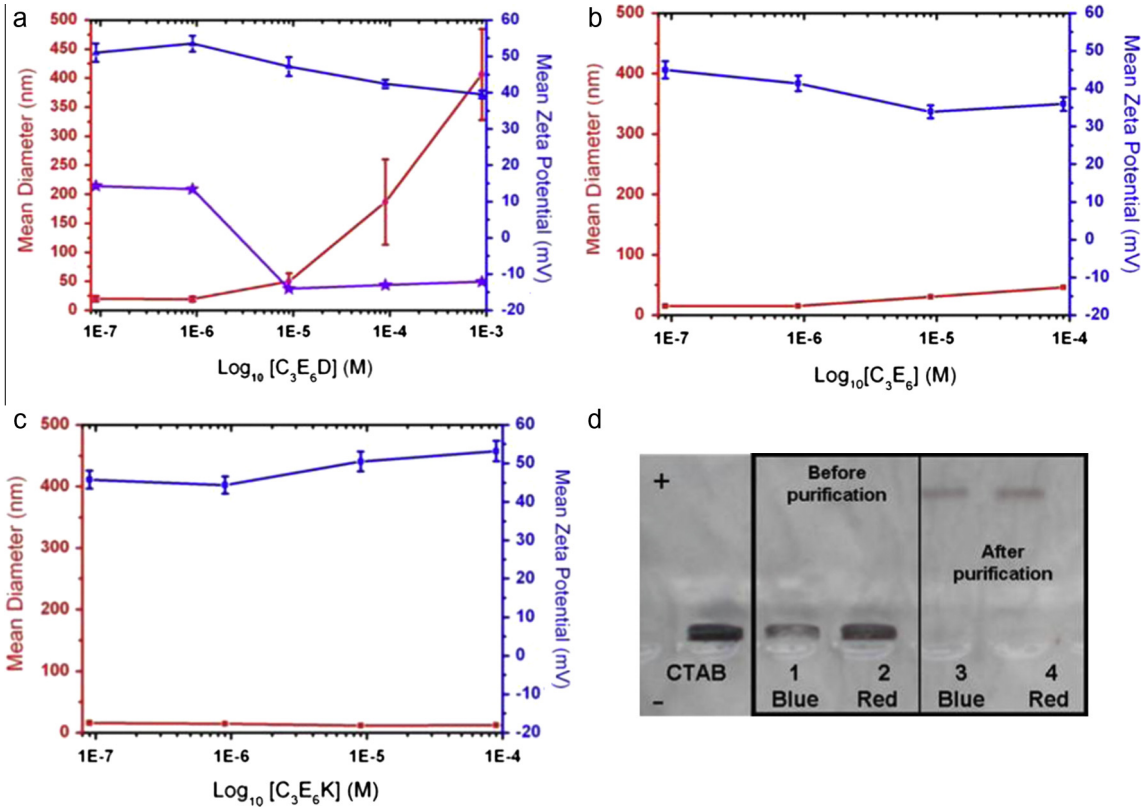

Fig. 3. Titration of a CTAB GNRs suspension (10^{-9} M) with a solution of 10 mM peptide: evolution of the mean diameter (red) and the zeta potential before purification on size exclusion column (blue) and after (purple): (a) negatively charged short C_3E_6D; (b) neutral charged C_3E_6 peptide; (c) positively charged C_3E_6K peptide; (d) image of the electrophoresis 0.5% agarose gel in TBE buffer and loaded with GNRs capped C_3E_6D exhibiting a blue-shift (lane 1 and 3) or a red-shift (lane 2 and 4) in absorbance spectrum respectively: (lane 1–2) before purification and (lane 3–4) after purification on size exclusion column. An electrical field of $E = 3.3$ V cm^{-1} was applied during 45 min for the migration. These experiments have been performed after and incubation time of 24 h with peptidic ligands. (For interpretation of the references to color in this figure legend, the reader is referred to the web version of this article.)

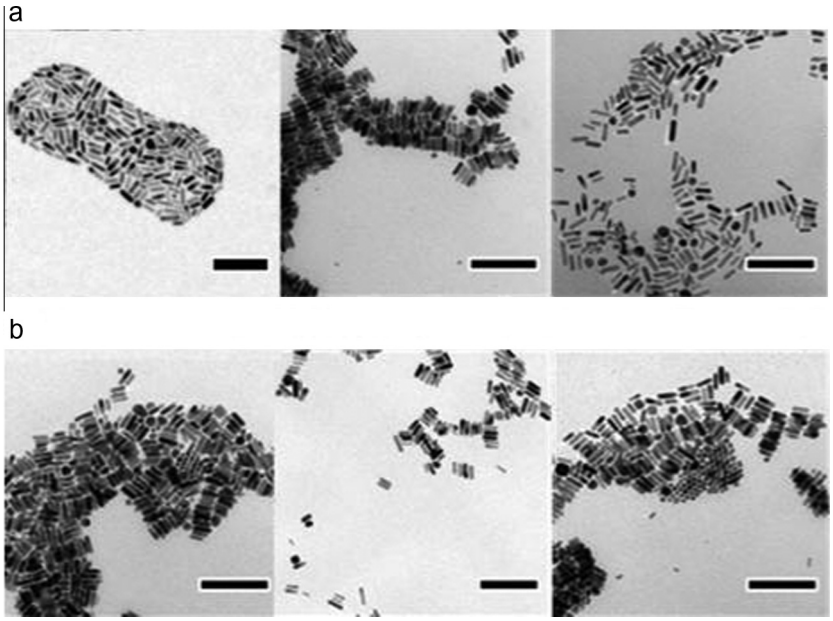

Fig. 4. Typical TEM images of GNRs during their titration with C_3E_6D peptide. (a) Blue-shifted sample (low concentration of peptide) and (b) red-shifted sample (high concentration of peptide). The scale bar represents 100 nm. The TEM grids have been prepared after an incubation time of 24 h with peptidic ligands.

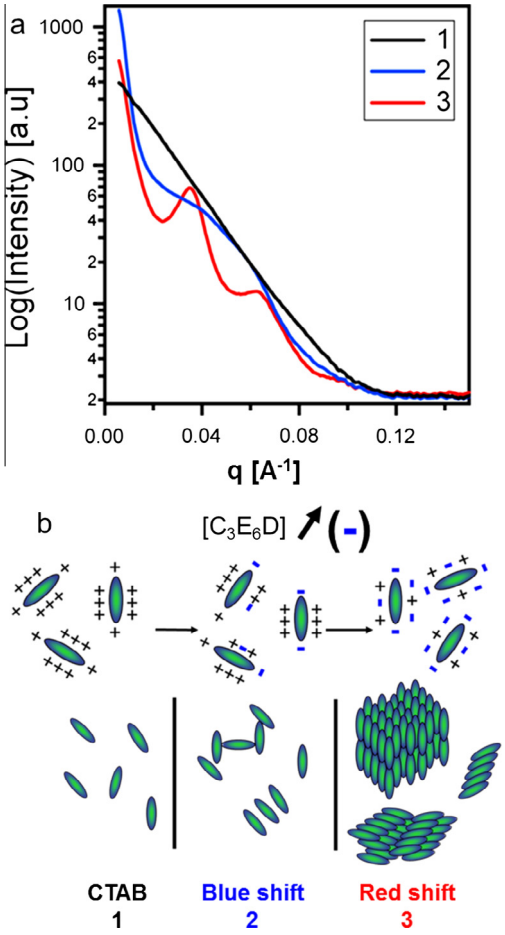

Fig. 5. (a) SAXS spectra of GNRs capped with CTAB (1, black) C_3E_6D peptide for a blue-shifted (2, blue) sample C_3E_6D peptide for a red-shifted sample (3, red). (b) Schematic view of the surface charge and the GNRs assemblies during the ligand exchange with short negatively charged peptides. The SAXS measurements have been performed after an incubation time of 5 days with the peptidic ligand. (For interpretation of the references to color in this figure legend, the reader is referred to the web version of this article.)

shaped nanoparticles can align in different ways either in an end-to-end fashion or in a parallel side-to-side manner. Their relative orientation affects plasmon couplings between the GNRs and therefore their optical absorption spectra. The side-to-side geometry generally leads to a blue-shift of the LSPR and a red-shift of the TSPR whereas the end-to-end geometry induces a red-shift of the LSPR [3b]. The plasmonic couplings between GNRs in other geometries have been widely investigated either by computer simulation and experimental studies [3b,c,15,19,24]. Typical images obtained from Transmission Electronic Microscopy (TEM) of blue-shifted and red-shifted aggregates are shown in Fig. 4a and b respectively. In both cases, the GNRs self-assembled into aggregates including several ten of nanoparticles. They have a tendency to self-assemble in a side-to-side manner with a regular stacking lateral interdistance of 3 nm. This small value is in agreement with the fact that CTAB bilayers are replaced with peptides at the surface of the GNRs. In the case of CTAB coated GNRs, the interdistance was found to be around 4 nm. In both cases, aggregates with an end-to-end tendency are also easy to observe. It is then difficult here to discriminate any difference in the structures of the blue-shifted and red-shifted GNRs self-assemblies. One has to notice that the sample preparation used implies a drying step that could disturb the initial organization of the GNRs in colloidal suspension.

To overcome this difficulty we used SAXS technique to identify the structural properties of the nanoparticles self-assemblies [4]. We investigated the samples by SAXS without any drying step. The experiments on a high brilliance beam line were performed on blue-shifted and red-shifted C_3E_6D GNRs suspensions in ~1.5 mm diameter glass capillaries, the particle concentration being 10^{-8} M. As a control, in the case of CTAB GNRs (trace 1, Fig. 5a), no peak was observed, which is in agreement with the fact that the GNRs are well dispersed in water. In the case of the blue-shifted C_3E_6D GNRs suspension (trace 2, Fig. 5a), a peak with an important curve slope around 0.0065 $Å^{-1}$ indicated the presence of amorphous aggregates in solution without ordering in solution. In contrast in the case of the red-shifted C_3E_6D GNRs suspension (trace 3, Fig. 5a), two Bragg peaks associated with respectively spacing of 18.5 nm ± 1 nm and 10 nm ± 1 nm respectively were observed. The latter spectrum is in agreement with the presence of larger aggregates with a better structuration.

To get further information about those disordered aggregates giving rise to a blue-shifted Longitudinal Surface Plasmon peak, typical TEM images of the blue-shifted sample were analyzed by using Fast Fourier Transform (FFT) (Fig. S8 in supplementary materials). Typical TEM images obtained from the blue shifted sample are shown in Fig. S8, exhibiting amorphous little aggregates (S8-1), well organized aggregates (S8-2), dispersed GNRs (S8-3) and large amorphous aggregates (S8-4). These images were analyzed by using Fast Fourier Transform (FFT) performed by open access software (Image J). The resulting circular integration was compared to the experimental data obtained from SAXS (labeled as raw data in Fig. S8). The FFT of TEM images give 2D information about the nanoparticle organization whereas SAXS data concern nanoparticles structuration in the volume of several μm^3 fixed by the beam size. Nevertheless it is noteworthy that the FFT profile gives a bump around the same position than the SAXS intensity profile (see Fig. S8). The best fitting with the SAXS data corresponds to the GNR arrangement shown in image 1 (Fig. S8).

The experiments are in agreement with the following mechanism for the nanorods assembling during the CTAB replacement with C_3E_6D (scheme in Fig. 5b). The "as synthetized" CTAB GNRs are initially positively charged and well-dispersed in solution (1 in Fig. 5b). As the peptide concentration increases in solution, small aggregates are formed due to attractive interaction between positive and negative ligand patches on the NR surface and the LSPR is blue-shifted (2 in Fig. 5b). The aggregates are amorphous, probably composed of rods assembled either in a side-by-side and "L" geometry and possess a weaker mean positive surface charge. As CTAB is progressively replaced with the negatively charged peptide, electrostatic attraction between nanorods becomes possible and therefore larger aggregates are formed giving rise to larger organized Smectic-like structures. The evolution of the optical properties during the ligand exchange is attributed to the interplay between plasmon couplings in the side-by-side and end-to-end geometry. Thus we demonstrated that the C_3E_6D ligands can replace the initial CTAB ligands and induce the formation of aggregates whose morphology and size depend on the peptide concentration.

3.4. Investigation of the structure obtained with the longer peptides

In view to optimize the chemical structure of the ligands, we finally compared the ligand exchange process performed with peptidic ligands bearing an undecanoyl chain ($C_3A_{11}E_4CO_2H$ and $C_3A_{11}E_4$, see Fig. 1c) or not (C_3E_6D). Interestingly, whatever the nature of the peptide, no aggregation was observed during the titration (See Fig. S9a and S9b). Meanwhile the mean surface charge of the nanorods decreased as the observed zeta potential. For high amount of peptides added, the zeta potential reached a value of −14 mV for $C_3A_{11}E_4CO_2H$ and −8 mV for $C_3A_{11}E_4$. After removal

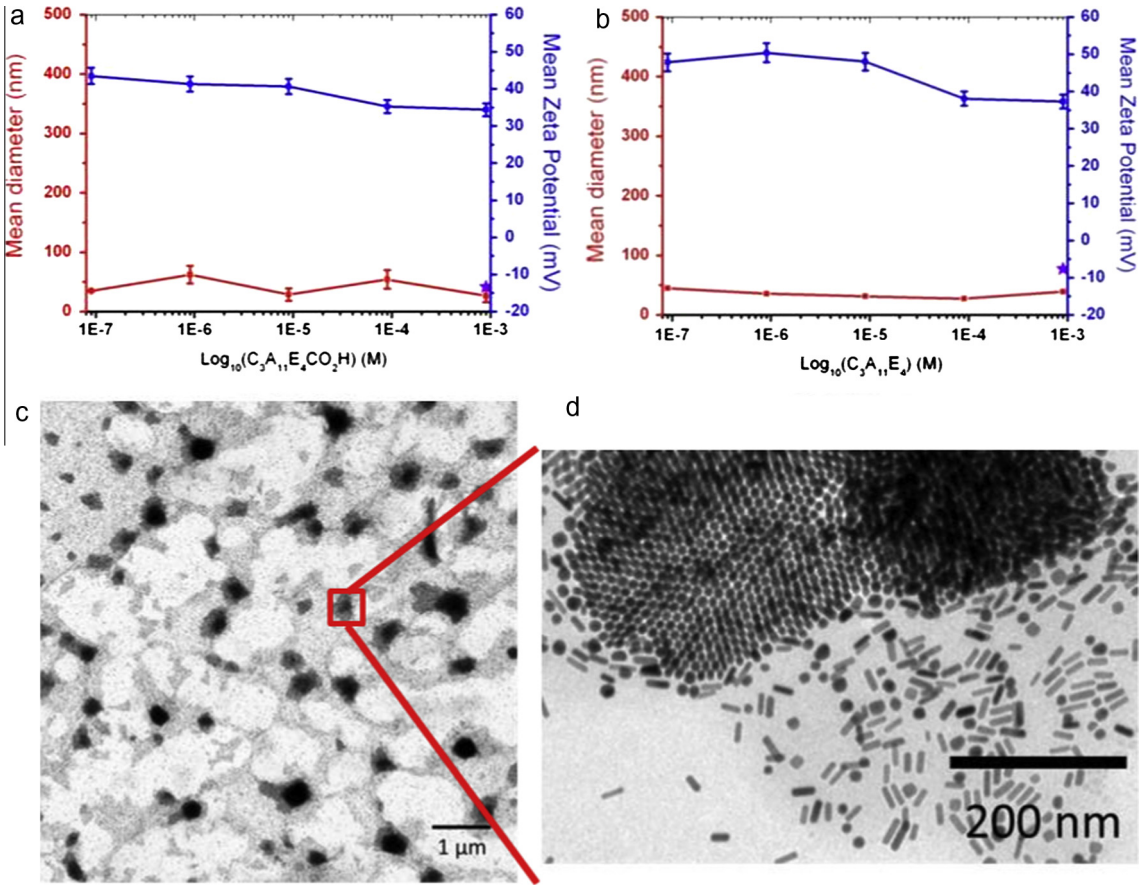

Fig. 6. Evolution of the mean diameter and the zeta potential during the titration of a CTAB GNRs suspension (10^{-9} M) with a solution of 10 mM peptide: (a) negatively charged $C_3A_{11}E_4CO_2H$ peptide; (b) neutral $C_3A_{11}E_4$. (c) Typical TEM image of GNRs capped with $C_3A_{11}E_4$, (d) zoom of one part of the previous image. The TEM grids have been prepared after an incubation time of 24 h with peptides.

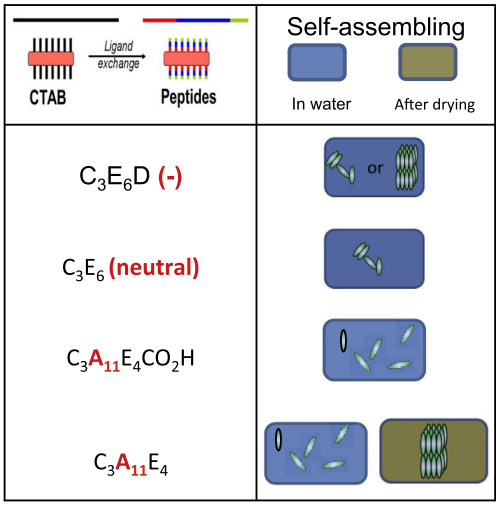

Fig. 7. Schematic view summarizing the effect of CTAB replacement with peptidic ligands at the GNRs surface and their self-assembling properties. Two sets of peptidic ligands have been used, denoted either short or long with an undecanoyl chain (short: C_3E_6D, C_3E_6 and C_3E_6K; long: $C_3A_{11}E_4CO_2H$, $C_3A_{11}E_4$).

of the ligand excess, these values are close to the zeta potential of C_3E_6D GNRs (−12 mV) measured after the purification step. To complete the characterization of these peptide GNRs, we investigated the colloidal stability of the GNRs after purification step on size column chromatography (see Fig. S9). Here we compared the results obtained for $C_3A_{11}E_4$, $C_3A_{11}E_4CO_2H$ and C_3E_6D by UV–Vis spectroscopy and DLS. All types of GNRs were well dispersed in solution over one week, after what aggregation was observed for $C_3A_{11}E_4$ and C_3E_6D. The best colloidal stability was demonstrated for $C_3A_{11}E_4CO_2H$. This experiment is in agreement with a higher surface concentration of the $C_3A_{11}E_4CO_2H$ ligands due to a better replacement of the initial CTAB ligands. Therefore colloids coated with $C_3A_{11}E_4CO_2H$ appear to be particularly appropriated for applications requiring a well-dispersed suspension of aqueous GNRs. Indeed, the slow drying of a GNRs suspension coated with $C_3A_{11}E_4$ peptide on a TEM grid resulted in a well-defined organization in TEM (see Fig. 6c and d and also Fig. S10). GNRs self-assembled in a hexagonal packing where GNRs relied perpendicular to the TEM grid. We also previously described highly ordered superlattices obtained by coating the GNRs with an undecanoyl PEGylated thiolate [4,25]. The $C_3A_{11}E_4$ ligand is close to this previous undecanoyl PEGylated thiolate in term of chemical structure. Only the anchor group composed here of three cysteins is different. This latter experiment permits to optimize the design of the ligand to obtain nanostructured superlattices. Here, the alkyl chain and the hydrophilic PEGylated spacer were found to play a crucial role to obtain gold nanorods superlattices [26].

4. Conclusion

We investigated in details the replacement of CTAB with peptidic ligands to chemically graft the gold nanorods surfaces. In this paper, we used different peptidic derivatives composed of an anchor group (three cysteins), a hydrophilic spacer and different

charged terminal groups (positive, negative and neutral) and with a biotin. The biotin peptide illustrates the possibility to graft more specifically targeting peptides. Furthermore, we were able to control the GNRs assembly either in solution or during drying by using short and long PEGylated peptidic ligands respectively (see Fig. 7). During the ligand exchange with short C_3E_6D peptide, self-assembling of the GNRs occurs by electrostatic interaction as the negatively charged peptides bound on the GNRs surface interact with the CTAB attached on another GNR. Furthermore the structure of the self-assembled aggregates obtained by SAXS was correlated to the change in optical properties. This experiment revealed organized smectic-like structures for large aggregates corresponding with a red shift of the LSPR band. Whereas smaller aggregates are amorphous as found by SAXS experiments corresponding to a blue shift of the LSPR band. Finally, the chemical structure of the peptides was adjusted by introducing an undecanoyl chain as additional spacer ($C_3A_{11}E_4CO_2H$ and $C_3A_{11}E_4$) to enhance the colloidal stability of the obtained GNRs making them attractive for any application requiring well-dispersed GNRs in the absence of CTAB. Moreover, the GNRs coated with $C_3A_{11}E_4$ can form well-defined superlattices by drying and are therefore good candidates as building blocks to design optical materials.

Funding sources

The Centre National de la Recherche Scientifique (CNRS), the Direction Générale de l'Armement (DGA) and the Région Bretagne supported the research described in this manuscript.

Acknowledgments

VM and FA thank the region Bretagne and the Direction Générale de l'Armement for the PhD fellowship of TB and CH. VM acknowledges the Agence Nationale de la Recherche for financial support through the biomodulator grant obtained in 2008 on the PNano program. We are indebted to A. Burel for her technical support during observations on the TEM platform Mric-UMS 3480-biosit-université de Rennes 1.

Appendix A. Supplementary material

Supplementary data associated with this article can be found, in the online version, at http://dx.doi.org/10.1016/j.jcis.2014.03.002.

References

[1] (a) S. Link, M.A. El-Sayed, J. Phys. Chem. B 103 (1999) 8410–8426;
(b) S. Link, M.A. El-Sayed, Annu. Rev. Phys. Chem. 54 (2003) 331–366.
[2] (a) B. Nikoobakht, Z.L. Wang, M.A. El-Sayed, J. Phys. Chem. B 104 (2000) 8635–8640;
(b) L. Onsager, Ann. N. Y. Acad. Sci. 51 (1949) 627–659;
(c) K. Liu, N. Zhao, E. Kumacheva, Chem. Soc. Rev. 40 (2011) 656–671;
(d) C.J. Murphy, T.K. Sau, A.M. Gole, C.J. Orendorff, J. Gao, L. Gou, S.E. Hunyadi, T. Li, J. Phys. Chem. B 109 (2005) 13857–13870.
[3] (a) A. Lee, A. Ahmed, D.P. dos Santos, N. Coombs, J.I. Park, R. Gordon, A.G. Brolo, E. Kumacheva, J. Phys. Chem. C 116 (2012) 5538–5545;
(b) A.M. Funston, C. Novo, T.J. Davis, P. Mulvaney, Nano Lett. 9 (2009) 1651–1658;
(c) P.K. Jain, S. Eustis, M.A. El-Sayed, J. Phys. Chem. B 110 (2006) 18243–18253.
[4] C. Hamon, M. Postic, E. Mazari, T. Bizien, C. Dupuis, P. Even-Hernandez, A. Jimenez, L. Courbin, C. Gosse, F. Artzner, V. Marchi-Artzner, ACS Nano 6 (2012) 4137–4146.
[5] (a) J. Pérez-Juste, I. Pastoriza-Santos, L.M. Liz-Marzán, P. Mulvaney, Coord. Chem. Rev. 249 (2005) 1870–1901;
(b) A. Gole, C.J. Murphy, Chem. Mater. 16 (2004) 3633–3640;
(c) C.J. Murphy, L.B. Thompson, A.M. Alkilany, P.N. Sisco, S.P. Boulos, S.T. Sivapalan, J.A. Yang, D.J. Chernak, J. Huang, J. Phys. Chem. Lett. (2010) 2867–2875;
(d) X. Huang, S. Neretina, M.A. El-Sayed, Adv. Mater. 21 (2009) 4880–4910.
[6] (a) T.B. Huff, M.N. Hansen, Y. Zhao, J.-X. Cheng, A. Wei, Langmuir 23 (2007) 1596–1599;
(b) A.K. Oyelere, P.C. Chen, X. Huang, I.H. El-Sayed, M.A. El-Sayed, Bioconjugate Chem. 18 (2007) 1490–1497;
(c) M. Hanauer, S. Pierrat, I. Zins, A. Lotz, C. Sonnichsen, Nano Lett. 7 (2007) 2881–2885;
(d) H. Liao, J.H. Hafner, Chem. Mater. 17 (2005) 4636–4641.
[7] S. Pierrat, I. Zins, A. Breivogel, C. Sonnichsen, Nano Lett. 7 (2007) 259–263.
[8] (a) A. Wijaya, K. Hamad-Schifferli, Langmuir 24 (2008) 9966–9969;
(b) K. Mitamura, T. Imae, N. Saito, O. Takai, J. Phys. Chem. B 111 (2007) 8891–8898.
[9] (a) A. Gole, C.J. Murphy, Langmuir 21 (2005) 10756–10762;
(b) J. Huang, K.S. Jackson, C.J. Murphy, Nano Lett. 12 (2012) 2982–2987.
[10] (a) A. Guerrero-Martínez, J. Pérez-Juste, E. Carbó-Argibay, G. Tardajos, L.M. Liz-Marzán, Angew. Chem. Int. Ed. 48 (2009) 9484–9488;
(b) Y.N. Tan, J.Y. Lee, D.I.C. Wang, J. Am. Chem. Soc. 132 (2010) 5677–5686.
[11] A. Schmidtchen, M. Pasupuleti, M. Mörgelin, M. Davoudi, J. Alenfall, A. Chalupka, M. Malmsten, J. Biol. Chem. 284 (2009) 17584–17594.
[12] (a) R. Lévy, N.T.K. Thanh, R.C. Doty, I. Hussain, R.J. Nichols, D.J. Schiffrin, M. Brust, D.G. Fernig, J. Am. Chem. Soc. 126 (2004) 10076–10084;
(b) D. Bartczak, A.G. Kanaras, Langmuir 27 (2011) 10119–10123.
[13] (a) L. Maus, O. Dick, H. Bading, J.P. Spatz, R. Fiammengo, ACS Nano 4 (2010) 6617–6628;
(b) X. Huang, X. Peng, Y. Wang, Y. Wang, D.M. Shin, M.A. El-Sayed, S. Nie, ACS Nano 4 (2010) 5887–5896.
[14] (a) A.I. Dif, F. Boulmedais, M. Pinot, V. Roullier, M.I. Baudy-Floc'h, F.d.r.M. Coquelle, S. Clarke, P. Neveu, F. Vignaux, R.L. Borgne, M. Dahan, Z. Gueroui, V. Marchi-Artzner, J. Am. Chem. Soc. 131 (2009) 14738–14746;
(b) A. Dif, E. Henry, F. Artzner, M. Baudy-Floc'h, M. Schmutz, M. Dahan, V. Marchi-Artzner, J. Am. Chem. Soc. 130 (2008) 8289–8296.
[15] L.B. Wang, Y.Y. Zhu, L.G. Xu, W. Chen, H. Kuang, L.Q. Liu, A. Agarwal, C.L. Xu, N.A. Kotov, Angew. Chem.-Int. Ed. 49 (2010) 5472–5475.
[16] (a) E. Dujardin, L.-B. Hsin, C.R.C. Wang, S. Mann, Chem. Commun. (2001) 1264–1265;
(b) M.R. Jones, R.J. Macfarlane, B. Lee, J. Zhang, K.L. Young, A.J. Senesi, C.A. Mirkin, Nat. Mater. 9 (2010) 913–917.
[17] T.S. Sreeprasad, A.K. Samal, T. Pradeep, Langmuir 24 (2008) 4589–4599.
[18] T.S. Sreeprasad, T. Pradeep, Langmuir 27 (2011) 3381–3390.
[19] C.J. Orendorff, P.L. Hankins, C.J. Murphy, Langmuir 21 (2005) 2022–2026.
[20] T.A. Larson, P.P. Joshi, K. Sokolov, ACS Nano 6 (2012) 9182–9190.
[21] F. Hubert, F. Testard, O. Spalla, Langmuir 24 (2008) 9219–9222.
[22] (a) N.R. Jana, L. Gearheart, C.J. Murphy, Adv. Mater. 13 (2001) 1389–1393;
(b) N.R. Jana, Small 1 (2005) 875–882.
[23] J. Israelachvili, Interface and Surface Forces, Academic Press, 1991.
[24] P.K. Jain, M.A. El-Sayed, Chem. Phys. Lett. 487 (2010) 153–164.
[25] Y. Xie, S. Guo, Y. Ji, C. Guo, X. Liu, Z. Chen, X. Wu, Q. Liu, Langmuir 27 (2011) 11394–11400.
[26] D.A. Walker, K.P. Browne, B. Kowalczyk, B.A. Grzybowski, Angew. Chem. Int. Ed. 49 (2010) 6760–6763.